Solidification and Stabilization of Heavy Metal–Contaminated Industrial Site Soil Using KMP Binder

Wei-Yi Xia[1]; Ya-Song Feng[2]; Yan-Jun Du[3]; Krishna R. Reddy, F.ASCE[4]; and Ming-Li Wei[5]

Abstract: A new and innovative binder KMP is developed for solidification/stabilization (S/S) of soils contaminated with heavy metals such as lead (Pb), zinc (Zn), and cadmium (Cd). The KMP consists of acid-activated phosphate rock, monopotassium phosphate, and reactive magnesia. However, effectiveness and immobilization mechanisms of KMP in actual field contaminated soils have not been investigated. This study presents a systematic investigation of strength, leachability, and microstructural properties of KMP stabilized field clayey soil that has been contaminated with Pb, Zn, and Cd at a smelter site. Several series of laboratory tests are conducted that include unconfined compression tests (UCT), toxicity characteristics leaching procedure (TCLP), modified European Communities Bureau of Reference (BCR) sequential extraction procedure, mercury intrusion porosimetry (MIP), X-ray diffraction (XRD), scanning electron microscope (SEM), and energy dispersive spectroscopy (EDS) studies. The TCLP and UCT results show that the leached Pb, Zn, and Cd concentrations decrease while unconfined compressive strength and dry density of the stabilized soil increase with increasing binder content and curing time. The sequential extraction results indicate that large percentages of Pb, Zn, and Cd are transferred from the exchangeable fraction to residual fraction after the KMP stabilization. The pore-size distribution reveals that the mean diameters and volumes of interaggregate and intra-aggregate pores decrease with an increase in the KMP content. The XRD and SEM/EDS analyses demonstrate the formation of magnesium phosphate-based products and heavy metal phosphate-based products in the stabilized soil, and they are the primary mechanisms for strength increase and heavy metal immobilization, respectively. **DOI: 10.1061/(ASCE)MT.1943-5533.0002264.**

Author keywords: Contaminated soil; Leachability; Microstructure; Pore-size distribution; Solidification/stabilization; Unconfined compressive strength.

Introduction

Heavy metal contamination in soils at industrial sites is of increasing concern in both developed and developing countries because of its potential threat to public health and detrimental effects on ecosystems (Reddy and Adams 2015). In addition, heavy metal contamination induces negative effects on mechanical characteristics of soils, resulting in unfavorable conditions for the redevelopment of these contaminated sites (Xue et al. 2014). In China, with the rapid industrialization during last three decades, soils in most industrial and populous areas have been impacted by heavy metal contamination (Duan et al. 2016). It is reported that heavily-polluted industrial sites, abandoned industrial sites, and mining sites in China are contaminated by pollutants (Hu et al. 2010, 2011; Du et al. 2014a), particularly heavy metals such as lead (Pb), zinc (Zn), cadmium (Cd), nickel (Ni), and copper (Cu) (Zhang et al. 2015).

Among the available technologies, the stabilization/solidification (S/S) technology is preferred for the remediation of soils contaminated by heavy metals because of its easy implementation, effectiveness, low cost, and faster cleanup (Sharma and Reddy 2004; Paria and Yuet 2006; USEPA 2007; Du et al. 2014b). Portland cement (PC) is the commonly used binder for soil improvement (Puppala et al. 2006; Saride et al. 2013; Shen et al. 2016) and S/S remediation of heavy metal contaminated soils (USEPA 2000; Paria and Yuet 2006); however, previous studies have shown that PC has the following distinct disadvantages: (1) with high soil pH (i.e., alkaline condition), heavy metals such as Pb, Zn, and Cd precipitate as metal hydrated phases and metal hydroxides, but they have potential to gradually dissolve at comparatively high or low pH conditions (Glasser 1997; Malviya and Chaudhary 2006); (2) when exposed to the long-term external environmental conditions such as sulfate attack and freeze-thaw cycles, PC stabilized soils could yield significant increase in leached concentrations of heavy metals and also decrease in unconfined compressive strength (Shi and Spence 2004; Du et al. 2014b, c); and (3) elevated heavy metal (particularly Zn) concentrations substantially can retard the cement hydration, leading to deterioration of density, strength, and elastic moduli of PC stabilized soils (Du et al. 2014b).

Recently, a new alternative binder, KMP, has been developed and successfully demonstrated for S/S of soils spiked with Pb or

[1]Ph.D. Student, Jiangsu Key Laboratory of Urban Underground Engineering and Environmental Safety, Institute of Geotechnical Engineering, Southeast Univ., Nanjing 210096, China. E-mail: diguosj@163.com

[2]Ph.D. Student, Jiangsu Key Laboratory of Urban Underground Engineering and Environmental Safety, Institute of Geotechnical Engineering, Southeast Univ., Nanjing 210096, China. E-mail: fengyasongys@126.com

[3]Professor, Jiangsu Key Laboratory of Urban Underground Engineering and Environmental Safety, Institute of Geotechnical Engineering, Southeast Univ., Nanjing 210096, China (corresponding author). E-mail: duyanjun@seu.edu.cn

[4]Professor, Dept. of Civil and Materials Engineering, Univ. of Illinois, Chicago, IL 60607. E-mail: kreddy@uic.edu

[5]Research Associate, State Key Laboratory of Geomechanics and Geotechnical Engineering, Institute of Rock and Soil Mechanics, Chinese Academy of Sciences, Wuhan 430071, China; formerly, Ph.D. Student, Jiangsu Key Laboratory of Urban Underground Engineering and Environmental Safety, Institute of Geotechnical Engineering, Southeast Univ., Nanjing 210096, China. E-mail: weimingli830716@sina.com

Note. This manuscript was submitted on March 15, 2017; approved on October 31, 2017; published online on March 19, 2018. Discussion period open until August 19, 2018; separate discussions must be submitted for individual papers. This paper is part of the ***Journal of Materials in Civil Engineering***, © ASCE, ISSN 0899-1561.

Zn alone, and mixed Pb and Zn contaminants (Du et al. 2014a, 2016). The KMP consists of oxalic acid-activated phosphate rock ($Ca_5(PO_4)_3F$) ($K_{sp} = 10^{-60.62}$), monopotassium phosphate (KH_2PO_4), and reactive magnesia (MgO). It is shown that stabilization of soils spiked with Pb or Zn alone or mixed Pb and Zn using KMP binder leads to much lower leachability as well as ecotoxicity as compared to PC stabilizer (Du et al. 2014a). The mechanisms of Pb and Zn immobilization by the KMP binder have been investigated by Du et al. (2014a, 2016). The microstructural analyses show that the formed fluoropyromorphite ($Pb_5(PO_4)_3F$) ($K_{sp} = 10^{-71.6}$), hopeite ($Zn_3(PO_4)_2 \cdot 4H_2O$) ($K_{sp} = 1.2 \times 10^{-17}$), scholzite ($CaZn_2(PO_4)_2 \cdot 2H_2O$) ($K_{sp} = 10^{-34.1}$), and zinc hydroxide ($Zn(OH)_2$) ($K_{sp} = 1.6 \times 10^{-5}$) are the primary mechanisms for immobilization of Pb and Zn with the KMP (Du et al. 2014a). Although the effectiveness of KMP binder has been demonstrated for the soils spiked with Pb and Zn, its effectiveness for the actual polluted soils at the industrial sites has not been investigated. Moreover, the immobilization mechanisms in S/S of Cd using KMP have remained unidentified and need more detailed studies for confirmation.

The objectives of the present study are to investigate the strength and leachability of the KMP stabilized site soil contaminated with Pb, Zn, and Cd, and identify the immobilization mechanisms of these heavy metals, especially Cd, based on microstructural characterization. The effects of KMP content and curing time on the strength and leachability are discussed. The results of this study are useful for facilitating the use of S/S at actual heavy metal contaminated sites.

Materials and Methods

Materials

The soil tested in this study is collected from a Pb-Zn smelter contaminated site (36° 33′N, 104° 12′E) in Gansu Province, China. The smelter was established in 1996, producing 130,000 tons of Zn, 50,000 tons of Pb, and 365 tons of Cd annually. The soil is collected within the top 0.50 m of depth, stored in polyethylene bags, and transferred to the laboratory for sample processing. The soil is air dried and sieved through a 1-mm sieve. Its physicochemical properties are tested and the results are shown in Table 1.

Table 1. Main Physicochemical Properties of Contaminated Soil Used in the Study

Property	Value
Plastic limit, w_P (%)[a]	17.2
Liquid limit, w_L (%)[a]	33.3
Soil type[b]	CL
Specific gravity, G_s	2.73
Heavy metal concentration (mg/kg)[c]	
Zinc, Zn	17300
Lead, Pb	9710
Cadmium, Cd	2425
Grain size distribution (%)[d]	
Clay (<0.005 mm)	6.54
Silt (0.005–0.075 mm)	43.95
Sand (0.075–1 mm)	49.51

[a]Tests are performed as per ASTM D4318 (ASTM 2010).
[b]CL = low plasticity clay, based on the Unified Soil Classification System (USCS) (ASTM 2011).
[c]Complete dissolution of samples is performed by acid digestion method using a mixture of $HF/HNO_3/HClO_4/H_2O_2$ (Hernandez et al. 2003).
[d]Measured using a laser particle size analyzer Master-sizer 2000.

Table 2. Oxide Chemistry of Phosphate Rock and MgO Tested

Oxide chemistry[a]	Phosphate rock (%)	MgO (%)
Calcium oxide (CaO)	45.93	0.23
Aluminium oxide (Al_2O_3)	1.23	0.28
Magnesium oxide (MgO)	—	87.95
Phosphorus oxide (P_2O_5)	25.10	0.03
Potassium oxide (K_2O)	—	0.011
Silicon oxide (SiO_2)	6.14	0.28
Sulphate oxide (SO_3)	—	0.45
Fluorine (F)	2.35	—
Chlorine (Cl)	—	0.28
Loss on ignition (950°C)	13.12	9.87

[a]Mineral composition is analyzed by X-ray fluorescence method using ARL9800XP + XRF spectrometry.

The KMP consists of 25% acid activated phosphate rock ($Ca_5(PO_4)_3F$), 25% monopotassium phosphate (KH_2PO_4) (chemical analytical reagent), and 50% of reactive magnesia (MgO) (industrial reagent) by weights (Du et al. 2014a, 2016). Commercial phosphate rock is used, and the major chemical compositions of commercial phosphate rock and MgO are listed in Table 2. Prior to the KMP binder preparation, the phosphate rock core is crushed and ground to pass through a sieve with 0.075 mm mesh, then mixed with 1.0 mol/L oxalic acid at a liquid–solid ratio of 2:1 for 5 min. After equilibration in a top-sealed vessel at 28 ± 1°C for 4 days, the mixture is oven dried at 60°C and passed through a 0.075 mm sieve until a final acid activated phosphate rock is obtained (Du et al. 2016).

Soil Sample Preparation

To prepare stabilized soil samples, deionized water is added to the air-dried soil to yield target water content of 22%. The water content in this study is defined as the ratio of the weight of the water to that of the total solid weight including binder and oven-dried soil (105 °C for 24 h). The KMP binder is then added to the rehydrated soil in four different amounts: 0 (i.e., untreated), 6, 8, and 10% (dry KMP weight to dry soil weight), and the soil-water-binder mixture is mixed for 5 min using an electric mixer to achieve homogeneity, and then transferred into a cylindrical mold with diameter of 50 mm and height of 100 mm (Arulrajah et al. 2016). Then, the mixture is statically compacted using a hydraulic jack to result in the desired dry density (1.51×10^3 kg/m^3) and water content (22%), which are the same as the maximum dry density and optimum water content of the untreated soil. The soil is then carefully extruded from the mold, wrapped with a polythene bag, and cured at 95% relative humidity and 22°C.

X-ray diffraction (XRD), scanning electron microscope (SEM), and energy dispersive spectroscopy (EDS) studies are conducted to understand the primary mechanisms of Cd immobilization by the KMP using KMP paste spiked with 12% Cd, as well as the Cd immobilization mechanisms in the stabilized soil affected by the coexisting Pb and Zn using 10% KMP stabilized soil. To prepare the KMP paste, predetermined volume of concentrated $Cd(NO_3)_2 \cdot 4H_2O$ (analytical reagent) solution is added to the KMP binder powder with predetermined weight until the water–binder ratio is approximately 2.4:1 and 12% Cd concentration is reached (i.e., Cd weight to binder weight). The mixture is mixed thoroughly using an electric mixer for approximately 5 min and then poured into a PVC mold with 50 mm in diameter and 100 mm in height. The PVC mold is wrapped with polythene caps and cured under controlled ambient condition (22°C and 95% relative humidity)

for 28 days. The mold is then removed and the specimen is subjected to XRD analysis.

However, XRD analysis of minerals containing Pb, Zn, and Cd formed in KMP stabilized soil is hindered by the low concentrations of Pb, Zn, and Cd elements in the site soil. Therefore, metal nitrates are used as the additional pollutant sources for Pb, Zn, and Cd to spike the field-contaminated soil. Correspondingly, 10% KMP stabilized spiked soil used for XRD observation is prepared and cured according to the similar procedure as described earlier in the preparation of KMP stabilized soil, with the exception that before the addition of KMP binder, analytical grade $Pb(NO_3)_2$, $Zn(NO_3)_2 \cdot 6H_2O$, and $Cd(NO_3)_2 \cdot 4H_2O$ solutions with predetermined concentrations and volumes are blended into the air-dried soil until both the water content of 22% and spiked Pb, Zn, Cd concentrations of 40,000 mg/kg each are achieved.

After 3, 7, 14, and 28 days of curing, the weight and volume of the stabilized soil samples are measured to determine the wet density. Various tests including unconfined compression tests (UCT), toxicity characteristics leaching procedure (TCLP), modified European Communities Bureau of Reference (BCR) sequential extraction procedure, and mercury intrusion porosimetry (MIP) are conducted on these samples to determine the unconfined compressive strength (q_u), metal leachability, metal speciation, and pore-size distribution, respectively. Specifically, cubic portions of approximate $1 \times 1 \times 1$ cm with fresh face at each side are carefully sampled from the UCT broken specimen, and are frozen using liquid nitrogen (−195°C) to be dried by sublimation of the frozen water at −80°C in a freezing unit with a vacuum chamber. The freeze-dried soil samples are then subjected to the MIP and SEM/EDS analyses. In addition, after 28 days of curing, 10% KMP stabilized spiked soil and KMP paste containing Cd are hand-broken to small pieces, and approximately 10 g is sampled, freeze-dried, ground, sieved (<0.075 mm) and subjected to the XRD analysis.

The KMP content, curing time, and the number of identical samples subjected to various tests are summarized in Table 3.

Testing Methods

The UCT is performed as per ASTM D4219 (ASTM 2008) with a constant strain rate of 1%/min. The coefficient of variation (COV) values of the measured q_u for three identical samples are less than 3.2%, showing the repeatability of the results. After UCT, small portions of the tested samples are immediately used for water content measurement as per ASTM D4219 (ASTM 2008) in order to determine the dry density.

The leaching test is conducted as per TCLP-EPA Method 1311 (USEPA 1992) in which the extraction fluid with a pH of 4.93 ± 0.05 (glacial CH_3COOH and NaOH diluted in water) is used. Approximately 10 g of soil sampled from each of the three identical UCT broken samples is air-dried, ground to pass through a 9.5 mm sieve, and then mixed with 200 mL of extraction fluid in a plastic container. After 18 h of mixing with a speed of 30 rpm in shaking mixer, the leachate in each container is then separated from the solid phase using a 0.4 μm glass fiber filter. Before analyzing the metal concentration using the inductively coupled plasma mass spectrometer (ICP-MS), all leachate samples are acidified with 1 N nitric acid to keep a pH of less than 2.

The modified BCR three-step sequential extraction procedure is conducted as per Du et al. (2016) to investigate metal chemical speciation. Approximately 10 g soil obtained from the UCT broken sample is air-dried, crushed, and passed through a 2 mm sieve first and then used for the sequential extraction testing. The sequential extraction procedure consists of four extraction steps, which determine the exchangeable fraction (F1), reducible fraction (F2), oxidizable fraction (F3), and residual fraction (F4) of Pb, Zn, and Cd in the samples tested.

The MIP test is performed using AutoPore IV 9510 mercury intrusion porosimeter capable of generating pressure in the range of subambient to 413 MPa. The pore diameter is calculated using the following capillary pressure equation (Horpibulsuk et al. 2009):

$$d = -\frac{4\tau \cos \alpha}{p} \tag{1}$$

where d = pore entry diameter in which mercury is being intruded (μm); τ = surface tension (N/m); α and p = contact angle of mercury with the solid (degrees), and applied pressure of mercury intrusion (MPa), respectively. In the present study, the contact angle and surface tension values are taken as 135° and 4.84×10^{-4} N/mm, respectively.

The XRD analysis is performed using a Rigaku D/Max-2500 X-ray diffractometer with Cu-Kα ($\lambda = 1.540538$ Å) radiation. An input voltage of 40 kV and a current of 20 mA are employed. Two-theta (2θ) value ranging between 5° and 70° with a step length of 0.02° and a scanning rate of 2°/min are used for samples scanning. The SEM/EDS test is conducted to observe the microstructure of stabilized soil surface. The dehydrated soil sample tested is coated with carbon before taking the SEM images. The SEM analysis is conducted using a LEO1530VP scanning electron microscope equipped with an energy dispersive X-ray spectroscopy (EDS) (INCA 300, Oxford Instruments).

Table 3. Binder Content and Curing Time of Samples for Various Tests

Test type[a]	Binder content (%)	Curing time (days)	Number of identical samples
Dry density	0, 6, 8, 10	3, 7, 14, 28	3
UCT	0, 6, 8, 10	3, 7, 14, 28	3
TCLP	0, 6, 8, 10	3, 7, 14, 28	3
BCR	0, 6, 8, 10	28	1
MIP	6, 8, 10	28	1
XRD	10[b] and KMP paste[c]	28	1
SEM/EDS	10	28	1

[a]BCR = modified European Communities Bureau of Reference sequential extraction procedure; EDS = energy dispersive spectroscopy; MIP = mercury intrusion porosimetry; SEM = scanning electron microscope; TCLP = toxicity characteristics leaching procedure; UCT = unconfined compression test; XRD = X-ray diffraction (XRD).
[b]10% KMP stabilized soil spiked with additional 40,000 mg/kg of Pb, Zn, and Cd.
[c]KMP paste containing 12% Cd.

Results and Discussion

Dry Density of Stabilized Soil

The dry densities of the stabilized soil samples are summarized in Fig. 1. It is shown that the mean dry density is 1.51×10^3 kg/m^3 for the untreated soil samples, and the KMP stabilization generally results in slightly higher dry density values for stabilized soil samples than those measured for the untreated soil samples. In addition, the stabilized soil exhibits a slight gradual increase of dry density with increasing KMP content and curing time. After 28 days of curing, the mean dry densities of stabilized soil samples increase from 1.63×10^3 to 1.69×10^3 kg/m^3 when the KMP content increases from 6 to 10%, which are 8 and 12% higher than those of untreated soil samples, respectively. The higher dry density of the

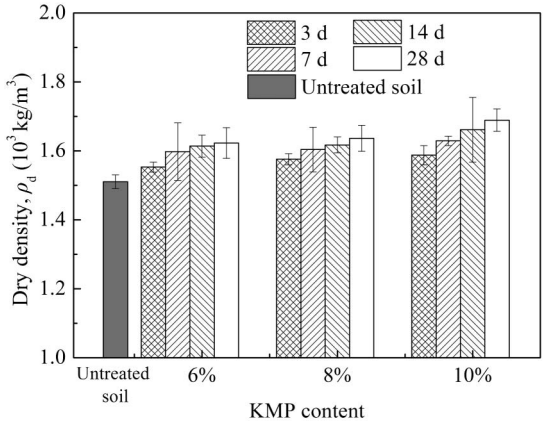

Fig. 1. Effect of KMP content on the dry density of the stabilized soil

KMP stabilized soil is attributed to the consumption of pore water and formation of the acid-base and hydration reaction products that fills the pore space in the soil matrix.

Unconfined Compression Test

Fig. 2 shows the variation of q_u with KMP content and curing time. It is shown that the stabilized soil has significantly higher q_u than the untreated soil, and q_u value increases with an increase in curing time. Generally, the q_u of the stabilized soil also increases with increasing binder content. For instance, when the binder content increases from 6 to 8% and 6 to 10%, q_u value of the KMP stabilized soil increases by approximately 1.7–2.1 times and 1.8–2.3 times after 7 and 28 days of curing, respectively. Note that when the KMP content is higher than 8%, the effect of binder content on q_u becomes moderate.

The increased strength of stabilized soil is attributed to the formation of the main reaction products of KMP: (1) struvite-(K) ($KMgPO_4 \cdot 6H_2O$, $K_{sp} = 2.4 \times 10^{-11}$) formed in the stabilized soil from an acid-base reaction possesses high chemical bonding strength, as reported by Du et al. (2014a), and thus provides greater resistance to compression; (2) unacidified reactive MgO remaining in the KMP could hydrate in the soil pore water to form magnesium hydroxide ($Mg(OH)_2$, $K_{sp} = 9.6 \times 10^{-4}$), and the formation of $Mg(OH)_2$ is associated with notable volume expansion and could subsequently further reinforce the soil structure and contribute to the strength (Xia et al. 2016); and (3) these products mentioned previously and other products, including farringtonite ($Mg_3(PO_4)_2$, $K_{sp} = 10^{-22.9}$), newberyite ($MgHPO_4 \cdot 3H_2O$, $K_{sp} = 10^{-5.8}$), and collinsite ($Ca_2Mg(PO_4)_2 \cdot 2H_2O$) could effectively fill large pore space, leading to a decrease in total pore volume and denser structure of soil with respect to KMP content, as discussed in detail in the section entitled "Pore-Size Distribution."

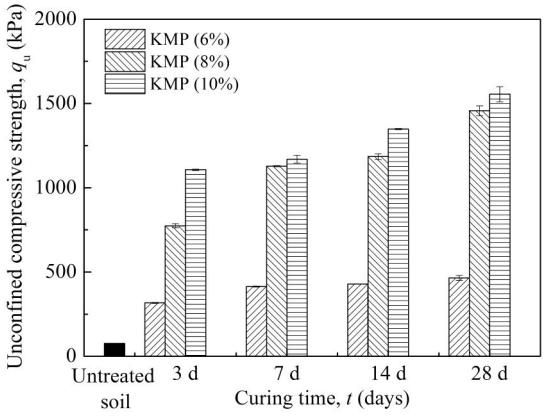

Fig. 2. Effect of curing time on unconfined compressive strength of KMP stabilized soil

TCLP Test

Fig. 3 shows the leached concentrations of heavy metals in the TCLP test. It is evident that the leached Pb and Cd concentrations of the untreated soil exceed the Resource Conservation and Recovery Act (RCRA) regulatory limits of 5.0 and 1.0 mg/L, respectively, indicating that the soil is hazardous and requires remediation. Furthermore, the average values of the Zn concentrations measured in the leachate is in excess of 800 mg/L. In contrast, the stabilized soil samples exhibit much lower leached concentrations of Pb, Zn, and Cd, and they decrease gradually with increasing curing time. For the stabilized soil samples at the curing time of 14 and 28 days, the leached Pb and Cd concentrations are below the RCRA regulatory limits, except for the soil with 6% KMP and 14 days of curing. It is shown that increasing KMP content significantly decreases the leached Pb, Zn, and Cd concentrations. After 28 days of curing, the lowest leached Zn concentration (0.11 mg/L) is observed for the case of 10% KMP, followed by 8% KMP (0.96 mg/L) and 6% KMP (1.18 mg/L). The leached Pb concentrations for the soil samples stabilized with 8 and 10% KMP are approximately one order of magnitude lower than that for the soil stabilized with 6% KMP. As for the leached Cd concentrations, they are dramatically reduced by 99% with KMP stabilization as compared to the untreated soil. This suggests chemical immobilization of Pb, Zn, and Cd using KMP provides an effective method for reducing metal leachability.

The decrease in leached metal concentrations of stabilized soil can be attributed to the following reasons: (1) formation of metal phosphate precipitates, which are highly insoluble and not susceptible to solubilization under acidic condition during the TCLP process; (2) the reduction of pH in the TCLP process is favorable for the dissolution of the remaining unacidified phosphate rock ($Ca_5(PO_4)_3F$) and release of a certain amount of phosphate (PO_4^{3-}) (Kanabo and Gilkes 1987; Elouear et al. 2008), which further promotes formation of metal phosphate precipitates. Increase in the curing time and binder content would result in substantial increase in the amount of metal precipitates, which correspondingly causes a decrease in leached metals (Wang 2008; Wang et al. 2014). Further detailed analysis of the mechanisms of Pb, Zn, and Cd fixation by KMP stabilization processes is made based on the results of chemical speciation, XRD, and SEM evidences (as detailed in the following sections).

Modified BCR Sequential Extraction

The results obtained by the modified BCR sequential extraction are shown in Table 4. Significant differences in heavy metals speciation are observed between the stabilized and untreated soils. Pb, Zn, and Cd are less mobile in the stabilized soil samples because of their lower F1 fraction contents and higher F4 fraction contents than the untreated soil. It is shown that the F1 fractions of Pb in the stabilized soil samples are 79–93% lower than the untreated soil sample. Approximately 38–47% of Zn in the stabilized soil samples is bound to the F4 fraction, while 24% of Zn is found in F4 fraction in the untreated soil. The F1 fraction content of Cd ranges from approximately 38–43% for the stabilized soil

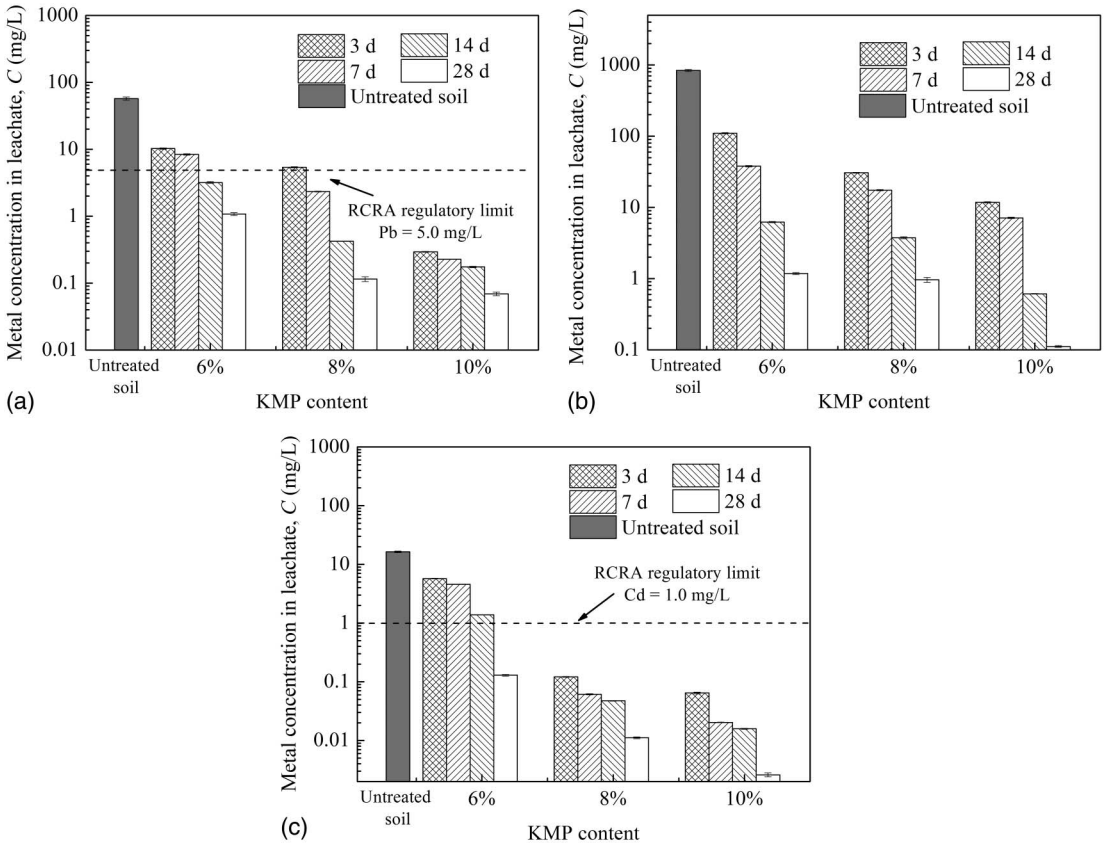

Fig. 3. Heavy metal concentration in TCLP leachate for KMP stabilized soil: (a) Pb; (b) Zn; (c) Cd

and is 78% for the untreated soil. Furthermore, the F1 fraction content decreases while that of F4 fraction increases with increasing KMP content. This result occurs because Pb, Zn, and Cd elements that are initially present in the F1 fraction (e.g., exchangeable Pb, Zn, and Cd) are strongly fixed to the metal phosphate precipitates after KMP stabilization. These metal precipitates include $Pb_5(PO_4)_3F$, zinc phosphate ($Zn_3(PO_4)_2$) ($K_{sp} = 10–35.3$), $CaZn_2(PO_4)_2 \cdot 2H_2O$, cadmium phosphate ($Cd_3(PO_4)_2$) ($K_{sp} = 10–32.6$), and cadmium phosphate hydroxide ($Cd_5(PO_4)_3OH$) ($K_{sp} = 10–64.62$), as well as calcium zinc hydroxide hydrate ($CaZn_2(OH)_6 \cdot 2H_2O$) ($K_{sp} = 10–43.9$), which can be further confirmed by XRD and SEM/EDS results. These Pb/Zn/Cd-bearing mineral precipitates are highly insoluble and immobile complexes, thus reducing exchangeable Pb, Zn, and Cd. It can be concluded that the KMP S/S results in the transformation of the F1 fractions of Pb, Zn, and Cd in contaminated soil into more insoluble residual fractions.

Table 4. Modified BCR Sequential Extraction Results for Zn, Pb, and Cd in KMP Stabilized Soil Sample after 28 Days of Curing

		Contaminant fraction (%)[a]			
Metal type	KMP content	F1	F2	F3	F4
Zn	Untreated soil	49.13	18.15	9.13	23.58
	6%	31.95	18.55	11.30	38.20
	8%	30.56	17.19	11.63	40.62
	10%	29.42	15.90	11.95	42.73
Pb	Untreated soil	38.61	44.37	16.11	0.92
	6%	7.95	38.19	28.44	25.42
	8%	5.38	36.46	30.73	27.43
	10%	2.84	34.16	32.70	30.30
Cd	Untreated soil	77.88	10.24	5.67	6.21
	6%	43.24	22.04	8.13	26.59
	8%	40.14	20.91	8.88	30.08
	10%	37.80	20.28	9.55	32.38

[a]F1 = exchangeable fraction; F2 = reducible fraction; F3 = oxidizable fraction; F4 = residual fraction.

Pore-Size Distribution

The internal structure represented by pore-size distribution plays a decisive role in influencing the physical and mechanical characteristics of stabilized soils (Horpibulsuk et al. 2009; Du et al. 2014b). Fig. 4(a) presents cumulative pore volume versus the entrance pore diameter of the KMP stabilized soil. It is shown that the soil stabilized with higher content of KMP has lower cumulative pore volume (i.e., void ratio). Fig. 4(b) shows the pore-size distribution (PSD) curves in terms of relationship between $dV/d\lg D$ and D, where V is the volume of mercury intruded at a given pressure increment corresponding to pores whose diameter is D. The area under the curve between any two pore diameters represents the volume of pores that are distributed between these two diameters (Horpibulsuk et al. 2009). It is shown in Fig. 4(b) that the area under the entire PSD curve decreases as the KMP content increases, which is attributed to the increase in acid-base and hydration reactions with KMP content (Du et al. 2014a). The distribution of PSD for each stabilized soil is bimodal with a major peak, and a minor but prominent peak.

Mathematically, a bimodal PSD curve, $f(D)$, can be fitted using the superposition of two overlapping unimodal pore-size distributions (Li and Zhang 2009; Du et al. 2014b). Therefore, a Gaussian

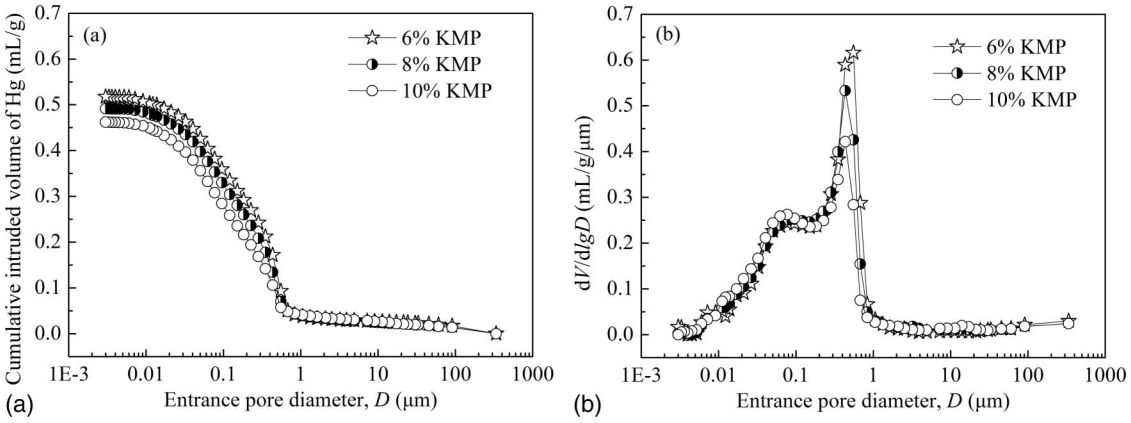

Fig. 4. MIP results for the KMP stabilized soil: (a) cumulative volume; (b) pore-size distribution

distribution function is applied to simulate each peak of the PSD curves as expressed by

$$f(D) = f_1(D) + f_2(D) = \frac{A_1}{w_1\sqrt{\pi/2}} \cdot e^{-\frac{2(\lg D-\mu_1)^2}{w_1^2}} + \frac{A_2}{w2\sqrt{\pi/2}} \cdot e^{-\frac{2(\lg D-\mu_2)^2}{w_2^2}} \quad (2)$$

where $f_1(D)$ and $f_2(D)$ = fitted curves for the minor and major peaks in the PSD curve on a logarithmic scale, respectively; μ_1 and μ_2 = mean pore diameters of minor and major peaks, respectively (μm); A_1 and A_2 = parameters indicating the pore volumes covered by $f_1(D)$ and $f_2(D)$, respectively (mL/g); and w_1 and w_2 = corresponding standard deviations on a logarithmic scale, respectively (μm).

Table 5 shows the values of parameter μ_1, μ_2, A_1, A_2, w_1, and w_2 obtained by regression analysis using the least square root method. Du et al. (2014b) indicate that the dual peaks in the PSD curves represent intra-aggregate and interaggregate pores of the stabilized zinc-contaminated clayey soil, respectively. It is shown in Table 5 that when the KMP content increases from 6 to 10%, μ_1 decreases from 0.114 to 0.092 μm (19% decrease) and μ_2 decreases also from 0.486 to 0.426 μm (12% decrease). When the KMP content increases from 6 to 10%, A_1 [the volume of an intra-aggregate pore covered by the simulated $f_1(D)$] slightly increases from 0.347 to 0.349 mL/g (0.6% increase) whereas A_2 [the volume of an interaggregate pore covered by the simulated $f_2(D)$] decreases considerably from 0.141 to 0.081 mL/g (43% decrease). Therefore, the reduction in the volume and mean pore diameter of interaggregate pores with KMP content, primarily contributes to the reduction in the total pore volume for KMP stabilized soil. The phenomenon is attributed to the enhanced KMP acid-base and hydration reactions and additional reaction products when KMP content increases. These reaction products include $Mg_3(PO_4)_2$, $MgHPO_4 \cdot 3H_2O$, $Mg(OH)_2$, $KMgPO_4 \cdot 6H_2O$, and $Ca_2Mg(PO_4)_2 \cdot 2H_2O$ formed in the stabilized soil that are able to fill in the large pore space between soil particles, resulting in significant reductions in volume of interaggregate pores. However, the increase in the quantity of acid-base and hydration reaction products does not considerably affect the filling of the pores within the soil particles. Hence, the changes in volume and size of intra-aggregate pores are not significant when the KMP content is increased.

The reduction in total pore volume with KMP content also coincides with the conclusions of the UCT and dry density analyses of the stabilized soil. As suggested by Ismail et al. (2002), a small decrease in pore volume is proved to be enough to generate a significant gain in strength because of the existence of a larger number of contacts between soil particles. Therefore, the dry density and q_u increase with increasing KMP content.

X-Ray Diffraction Analysis

The XRD results are presented in Fig. 5. For both the stabilized spiked soil and KMP paste, the presence of $Mg_3(PO_4)_2$ (2θ of 25.86° and 23.07°), $MgHPO_4 \cdot 3H_2O$ (2θ of 29.35° and 25.71°), $Mg(OH)_2$ (2θ of 38.02° and 18.59°), and $KMgPO_4 \cdot 6H_2O$ (2θ of 20.93° and 30.81°) is identified, which is also observed in KMP stabilized Pb or Zn contaminated soil reported by Du et al. (2014a, 2016). In addition, $Ca_2Mg(PO_4)_2 \cdot 2H_2O$ has also been identified at 2θ of approximately 29.36° and 33.38°, which is absent in the KMP stabilized Pb or Zn contaminated soil (Du et al. 2014a, 2016).

It is also evident that two Cd-bearing minerals are present in both the stabilized spiked soil and the KMP paste containing Cd. A strong and sharp peak is present at 2θ of 32.29°, attesting the formation of $Cd_5(PO_4)_3OH$; moreover, $Cd_3(PO_4)_2$ corresponding to 2θ of 27.08° has also been detected. In the stabilized spiked soil, formation of both Pb-bearing and Zn-bearing minerals is also observed. Two peaks at 2θ of 30.59° and 27.95° clearly appear, attesting the formation of $Pb_5(PO_4)_3F$. Furthermore, the characteristic peaks of $Zn_3(PO_4)_2$ (2θ of 25.92° and 20.34°), $CaZn_2(PO_4)_2 \cdot 2H_2O$ (2θ of 10.34°), and $CaZn_2(OH)_6 \cdot 2H_2O$ (2θ of 31.02° and 28.59°) in the stabilized spiked soil have been detected.

Table 5. Parameters Obtained from the Simulated PSD Curves of the KMP Stabilized Soil Samples Based on Peak Analysis

KMP content (%)	μ_1 (μm)	μ_2 (μm)	A_1 (mL/g)	A_2 (mL/g)	w_1 (μm)	w_2 (μm)	R^2
6	0.114	0.486	0.347	0.141	1.246	0.250	0.982
8	0.107	0.446	0.347	0.114	1.227	0.264	0.985
10	0.092	0.426	0.349	0.081	1.233	0.257	0.982

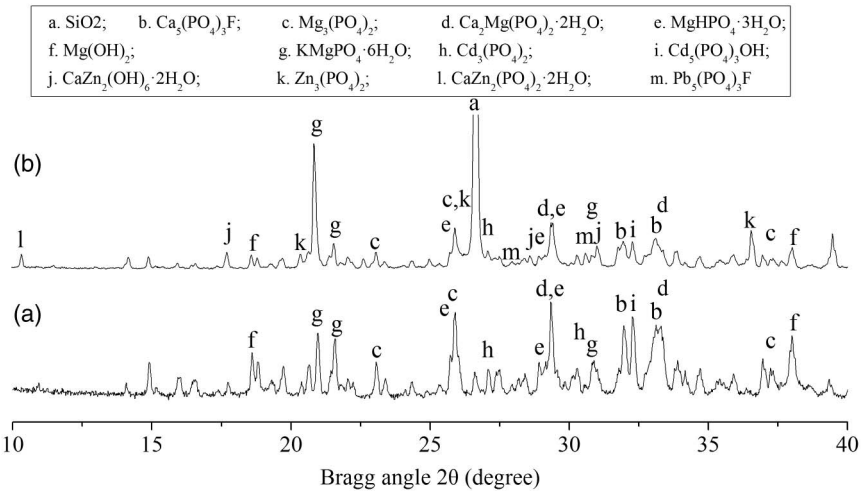

Fig. 5. X-ray diffractograms of the samples cured for 28 days: (a) KMP paste containing 12% Cd; (b) 10% KMP stabilized spiked soil

Scanning Electron Microscope and Energy Dispersive Spectroscopy Analysis

Fig. 6(a) presents SEM/EDS images of the 10% KMP stabilized soil, while Figs. 6(b–i) show the distribution maps of various elements including Pb, Zn, Cd, phosphorus (P), magnesium (Mg), calcium (Ca), potassium (K), and fluorine (F) for the 10% KMP stabilized soil. It is shown that massive segregated flake products are distributed at the surface of stabilized soil grain, which have been identified as $Mg_3(PO_4)_2$ (Aramendia et al. 1995), $MgHPO_4 \cdot 3H_2O$ (Sugiyama et al. 2009), $KMgPO_4 \cdot 6H_2O$ (Graeser et al. 2008; Nguyen et al. 2012; Du et al. 2014a), or $Ca_2Mg(PO_4)_2 \cdot 2H_2O$ (Onac et al. 2011) by overlapping the distribution maps of the Mg, P, and Ca [Figs. 6(e–g)]. The presence of a small quantity of $Pb_5(PO_4)_3F$ (Du et al. 2014a, 2016) has also been observed in the 10% KMP stabilized soil by overlapping the distribution maps for Pb [Fig. 6(b)], P [Fig. 6(e)], and F [Fig. 6(i)]. It is also observed that a certain quantity of cluster products, $CaZn_2(PO_4)_2 \cdot 2H_2O$ (Pokorny et al. 2012; Ban et al. 1999; Du et al. 2014a), $Zn_3(PO_4)_2$ (Calvo 1965; Stephens and Calvo 1967), and $CaZn_2(OH)_6 \cdot 2H_2O$ (Tong and Liu 2011) precipitates on the surface of the phosphate rock grain, as shown in Figs. 6(a, c, e, and g). The presence of $CaZn_2(PO_4)_2 \cdot 2H_2O$, $Zn_3(PO_4)_2$, and $CaZn_2(OH)_6 \cdot 2H_2O$ in the KMP stabilized soil is also substantiated by the XRD analysis (Fig. 5). In addition, it is evident that a large number of cluster products are highlighted by overlapping the distribution maps of Cd and P precipitated on

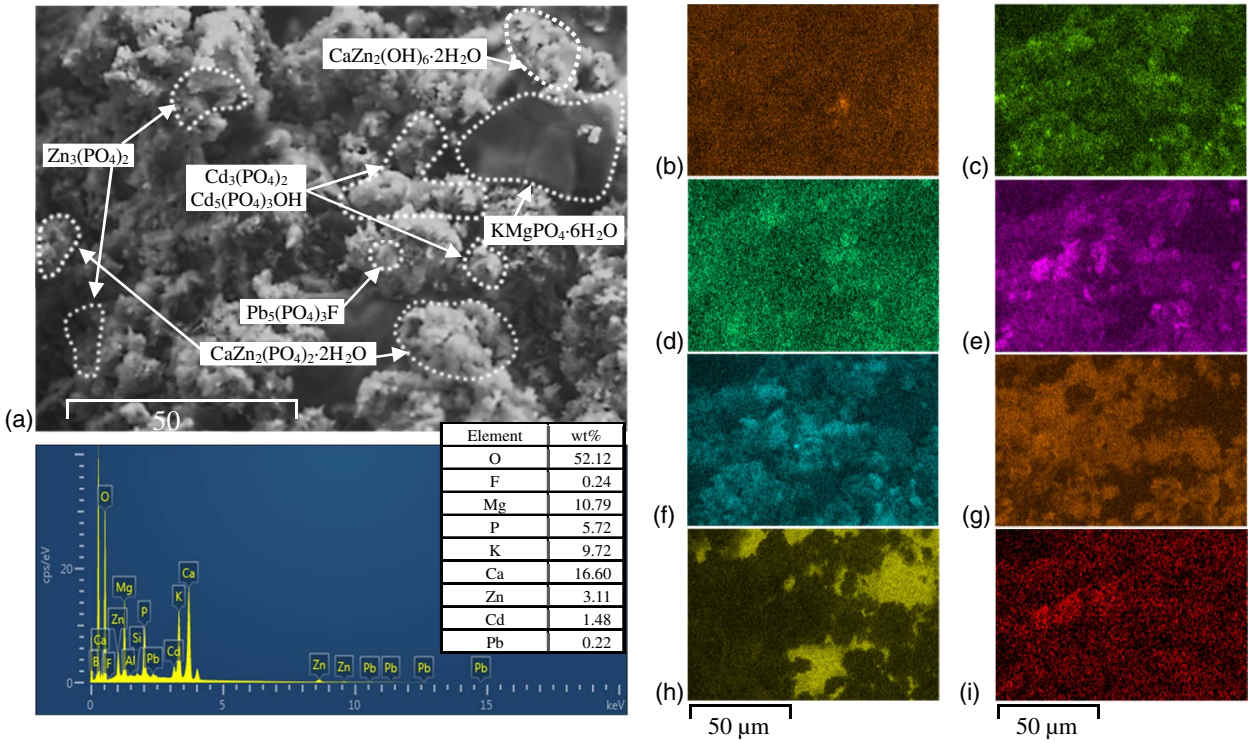

Fig. 6. SEM/EDS images of (a) the 10% KMP stabilized soil, and the distribution maps for different elements: (b) Pb; (c) Zn; (d) Cd; (e) P; (f) Mg; (g) Ca; (h) K; (i) F

the surface of the soil grain [Figs. 6(a, d, and e)], which are identified as $Cd_3(PO_4)_2$ (Matusik et al. 2008; Wacławska and Szumera 2011) and $Cd_5(PO_4)_3OH$ (Zhu et al. 2004; Guan et al. 2016) by the XRD analysis results shown in Fig. 5.

The previous results and discussions highlight the effectiveness of the KMP binder in metal immobilization and strength improvement of contaminated site soil, fully complying with the RCRA criteria for solid waste. Thus the stabilized soil is converted into a nonhazardous material as defined by RCRA and can be disposed of in a lined municipal solid waste (nonhazardous) landfill. Furthermore, because of the limited availability of solid waste disposal facilities and high cost of landfills, it is important to evaluate the possibility of reusing KMP stabilized soil and returning it to the economic mainstream as a resource material. In fact, the lower leachability and improved mechanical properties broaden the stabilized soil reuse applications, not only as a landfill liner or cover material but also as a resource material for other engineered applications such as a backfill for excavations, a roadway subgrade material, and even as a planting soil. Previous studies by the authors have shown that KMP binder (i.e., SS-B) can successfully transforms the Pb and Zn spiked soil into a functional material suitable for reuse as roadway subgrade backfill (Wu et al. 2015) and greening planting soil (Yu 2016). In terms of the KMP stabilized contaminated site soil in this study, further research is needed to evaluate its reuse applications and corresponding engineering properties (e.g., rebound modulus, water stability, and phytotoxicity).

Conclusions

From the results presented in this study, the following conclusions can be drawn:

- The dry density and q_u of the KMP stabilized soil increase with increasing binder content and curing time. The KMP can significantly reduce leached concentrations of Pb, Zn, and Cd as compared to the untreated soil. Increasing KMP content or curing time results in lower leachability. After 28 days of curing, all KMP stabilized soil samples meet the RCRA regulatory limits;
- When stabilized with higher KMP content, larger amounts of Pb, Zn, and Cd are transferred from exchangeable fraction (F1) to the residual fraction (F4). This result indicates that the KMP can change the metal speciation into a form that reduces metal leachability in the soil effectively;
- Contaminated soil stabilized with higher KMP content possesses smaller pore volume and size because of increased reaction products. A dual-porosity structure represented by interaggregate and intra-aggregate pores is found in each stabilized soil sample. The KMP stabilization can cause considerable reduction in the volume of the interaggregate pores, but only slightly affects the volume or mean diameter of intra-aggregate pores. The significant variations in the dry density and strength properties of the stabilized soil are well interpreted by the MIP analysis;
- The XRD and SEM/EDS analyses show that highly insoluble $Cd_3(PO_4)_2$ and $Cd_5(PO_4)_3OH$ are the primary products involved in the immobilization of Cd with KMP. Moreover, $Ca_5(PO_4)_3F$, $Mg_3(PO_4)_2$, $MgHPO_4 \cdot 3H_2O$, $Ca_2Mg(PO_4)_2 \cdot 2H_2O$, $Mg(OH)_2$, $KMgPO_4 \cdot 6H_2O$, and immobile Pb/Zn-bearing minerals including $Pb_5(PO_4)_3F$, $Zn_3(PO_4)_2$, $CaZn_2(PO_4)_2 \cdot 2H_2O$, and $CaZn_2(OH)_6 \cdot 2H_2O$ are also detected in the stabilized soil. This observation explains the reason for low leachability of Pb, Zn, and Cd in KMP stabilized soil; and
- The effects of KMP content on the leachability and strength of the stabilized soil are well interpreted based on the analyses of sequential extraction, XRD, and MIP results. However, additional microscopic tests are needed to further validate the effect of curing time on the microstructure characterization. In addition, additional research is warranted to extend the research findings to various types of contaminated soils (e.g., contaminated silty soils) and the reuse potential of stabilized soil for engineering applications such as roadway subgrade.

Acknowledgments

The authors are grateful for the support of National High Technology Research and Development Program of China (Grant No. 2013AA06A206), the State Key Program of National Natural Science of China (Grant No. 41330641), National Natural Science Foundation of China (Grant No. 41472258), and Environmental Protection Scientific Research Project of Jiangsu Province (Grant No. 2016031).

References

Aramendia, M. A., et al. (1995). "Modification of the activity of $Mg_3(PO_4)_2$ in the gas-phase conversion of cyclohexanol by addition of sodium-carbonate." *J. Catal.*, 157(1), 97–108.

Arulrajah, A., Kua, T. A., Horpibulsuk, S., Phetchuay, C., Suksiripattanapong, C., and Du, Y. J. (2016). "Strength and microstructure evaluation of recycled glass-fly ash geopolymer as low-carbon masonry units." *Constr. Build. Mater.*, 114, 400–406.

ASTM. (2008). "Standard test method for unconfined compressive strength index of chemical-grouted soils." *ASTM D4219*, West Conshohocken, PA.

ASTM. (2010). "Standard test methods for liquid limit, plastic limit, and plasticity index of soils." *ASTM D4318*, West Conshohocken, PA.

ASTM. (2011). "Standard practice for classification of soils for engineering purposes (Unified Soil Classification System)." *ASTM D2487*, West Conshohocken, PA.

Ban, S., Matsuo, K., Mizutani, N., and Hasegawa, J. (1999). "Hydrothermal-electrochemical deposition of calcium phosphates on various metals." *Dent. Mater. J.*, 18(3), 259–270.

Calvo, C. (1965). "The crystal structure of α-$Zn_3(PO_4)_2$." *Can. J. Chem.*, 43(2), 436–445.

Du, Y. J., et al. (2014a). "New phosphate-based binder for stabilization of soils contaminated with heavy metals: Leaching, strength and microstructure characterization." *J. Environ. Manage.*, 146, 179–188.

Du, Y. J., Jiang, N. J., Liu, S. Y., Jin, F., Singh, D. N., and Puppala, A. J. (2014b). "Engineering properties and microstructural characteristics of cement-stabilized zinc-contaminated kaolin." *Can. Geotech. J.*, 51(3), 289–302.

Du, Y. J., Wei, M. L., Reddy, K. R., Liu, Z. P., and Jin, F. (2014c). "Effect of acid rain pH on leaching behavior of cement stabilized lead-contaminated soil." *J. Hazard. Mater.*, 271, 131–140.

Du, Y. J., Wei, M. L., Reddy, K. R., and Wu, H. L. (2016). "Effect of carbonation on leachability, strength and microstructural characteristics of KMP binder stabilized Zn and Pb contaminated soils." *Chemosphere*, 144, 1033–1042.

Duan, Q., Lee, J., Liu, Y., Chen, H., and Hu, H. (2016). "Distribution of heavy metal pollution in surface soil samples in China: A graphical review." *Bull. Environ. Contam. Toxicol.*, 97(3), 303–309.

Elouear, Z., Bouzid, J., Boujelben, N., Feki, M., Jamoussi, F., and Montiel, A. (2008). "Heavy metal removal from aqueous solutions by activated phosphate rock." *J. Hazard. Mater.*, 156(1), 412–420.

Glasser, F. P. (1997). "Fundamental aspects of cement solidification and stabilisation." *J. Hazard. Mater.*, 52(2–3), 151–170.

Graeser, S., et al. (2008). "Struvite-(K), $KMgPO_4 \cdot 6H_2O$, the potassium equivalent of struvite-a new mineral." *Eur. J. Mineral.*, 20(4), 629–633.

Guan, W. F., Yan, T. J., Xiao, Y., Tian, J., Li, W. J., and You, J. M. (2016). "Design of cadmium hydroxyapatite hierarchical structures with adjustable morphology by a template-free hydrothermal route." *Chin. J. Struct. Chem.*, 35(7), 1059–1069.

Hernandez, L., Probst, A., Probst, J. L., and Ulrich, E. (2003). "Heavy metal distribution in some French forest soils: Evidence for atmospheric contamination." *Sci. Total. Environ.*, 312(1), 195–219.

Horpibulsuk, S., Rachan, R., and Raksachon, Y. (2009). "Role of fly ash on strength and microstructure development in blended cement stabilized silty clay." *Soils Found.*, 49(1), 85–98.

Hu, L. M., Meegoda, J. N., Du, J. T., Gao, S. Y., and Wu, X. F. (2011). "Centrifugal study of zone of influence during air-sparging." *J. Environ. Monit.*, 13(9), 2443–2449.

Hu, L. M., Wu, X. F., Liu, Y., Meegoda, J. N., and Gao, S. Y. (2010). "Physical modeling of air flow during air sparging remediation." *Environ. Sci. Technol.*, 44(10), 3883–3888.

Ismail, M. A., Joer, H. A., Randolph, M. F., and Meritt, A. (2002). "Cementation of porous materials using calcite." *Geotechnique*, 52(5), 313–324.

Kanabo, I. A. K., and Gilkes, R. J. (1987). "The role of soil pH in the dissolution of phosphate rock fertilizers." *Fert. Res.*, 12(2), 165–173.

Li, X., and Zhang, L. M. (2009). "Characterization of dual-structure pore-size distribution of soil." *Can. Geotech. J.*, 46(2), 129–141.

Malviya, R., and Chaudhary, R. (2006). "Leaching behavior and immobilization of heavy metals in solidified/stabilized products." *J. Hazard. Mater.*, 137(1), 207–217.

Matusik, J., Bajda, T., and Manecki, M. (2008). "Immobilization of aqueous cadmium by addition of phosphates." *J. Hazard. Mater.*, 152(3), 1332–1339.

Nguyen, K. S., Nguyen, P. V., Nguyen, H., Nguyen, T. N., and Nguyen, T. H. (2012). "Use of phosphate magnesium material in fire protection of concrete." *Proc., 5th Asian Concrete Federation Int. Conf.*, Asian Concrete Federation, Pathumthani, Thailand, 24–26.

Onac, B. P., Effenberger, H. S., Collins, N. C., Kearns, J. B., and Breban, R. C. (2011). "Revisiting three minerals from Cioclovina cave (Romania)." *Int. J. Speleol.*, 40(2), 99–108.

Paria, S., and Yuet, P. K. (2006). "Solidification-stabilization of organic and inorganic contaminants using portland cement: A literature review." *Environ. Rev.*, 14(4), 217–255.

Pokorny, P., Brozek, V., and Mastny, L. (2012). "Improving bond strength between carbon steel and plasma sprayed ceramic coatings through a phosphating process." *Conf. Proc., METAL 2012*, Tanger, Ostrava, Czech Republic, 69–70.

Puppala, A. J., Kadam, R., Madhyannapu, R. S., and Hoyos, L. R. (2006). "Small-strain shear moduli of chemically stabilized sulfate-bearing cohesive soils". *J. Geotech. Geoenviron. Eng.*, 10.1061/(ASCE)1090-0241(2006)132:3(322), 322–336.

Reddy, K., and Adams, J. (2015). *Sustainable remediation of contaminated sites*, Momentum Press, New York.

Saride, S., Puppala, A. J., and Chikyala, S. R. (2013). "Swell-shrink and strength behaviors of lime and cement stabilized expansive organic clays." *Appl. Clay Sci.*, 85, 39–45.

Sharma, H. D., and Reddy, K. R. (2004). *Geoenvironmental engineering: Site remediation, waste containment, and emerging waste management technologies*, Wiley, Hoboken, NJ.

Shen, S. L., Cui, Q. L., Ho, C. E., and Xu, Y. S. (2016). "Ground response to multiple parallel microtunneling operations in cemented silty clay and sand." *J. Geotech. Geoenviron. Eng.*, 10.1061/(ASCE)GT.1943-5606.0001441, 04016001.

Shi, C., and Spence, R. (2004). "Designing of cement-based formula for solidification/stabilization of hazardous, radioactive, and mixed wastes." *Crit. Rev. Environ. Sci. Technol.*, 34(4), 391–417.

Stephens, J. S., and Calvo, C. (1967). "Crystal structure of β-$Zn_3(PO_4)_2$." *Can. J. Chem.*, 45(20), 2303–2316.

Sugiyama, S., Manabe, T., Ioka, D., Nakagawa, K., Sotowa, K. I., and Shigemoto, N. (2009). "Removal of aqueous ammonium from industrial wastewater with magnesium hydrogen phosphate." *Phosphorus Res. Bull.*, 23, 15–19.

Tong, M., and Liu, X. (2011). "Preparation and characterization of calcium zincate synthesized by microwave method." *Environ. Eng. Manage. J.*, 10(7), 905–908.

USEPA (United States Environmental Protection Agency). (1992). "Toxicity characteristic leaching procedure (TCLP)." *Method 1311*, Washington, DC.

USEPA (United States Environmental Protection Agency). (2000). "Solidification/stabilization use at superfund sites." *EPA 542-R-00-010*, Office of Solid Waste and Emergency Response, Washington, DC.

USEPA (United States Environmental Protection Agency). (2007). "Treatment technologies for site cleanup: Annual status report, 12th Ed." *EPA 542-R-07-012*, Office of Solid Waste and Emergency Response, Washington, DC.

Wacławska, I., and Szumera, M. (2011). "Fosforanowe materiały ceramiczne do immobilizacji kadmu w środowisku glebowym." *Materiały Ceramiczne/Ceram. Mater.*, 63(2), 407–412.

Wang, B. L. (2008). "Mechanism Pb/Zn mining tailing contaminated soil remediation using phosphorus." Ph.D. thesis, Zhejiang Univ., Hangzhou, China (in Chinese).

Wang, J. R., Ma, B. G., and Li, X. G. (2014). "The solidification and hydration products of magnesium phosphate cement with Pb^{2+}, Zn^{2+} and Cu^{2+}." *J. Funct. Mater.*, 45(5), 5060–5064.

Wu, H. L., Wei, M. L., Du, Y. J., and Zhu, J. J. (2015). "Studies on the performances of stabilized Zn and Pb contaminated soils by a new phosphate-binder reuse as a subgrade backfill material." *Chin. Civil. Eng. J.*, 48(S2), 369–373 (in Chinese).

Xia, W. Y., Wei, M. L., Du, Y. J., Yu, B. W., and Song, D. J. (2016). "Experimental study on ex-situ S/S for shallow soil of organically contaminated site." *Chin. J. Geotech. Eng.*, 38(3), 510–517 (in Chinese).

Xue, Q., Li, J. S., and Liu, L. (2014). "Effect of compaction degree on solidification characteristics of Pb-contaminated soil treated by cement." *Clean Soil Air Water*, 42(8), 1126–1132.

Yu, B. W. (2016). "Study of the greening revegetation and long-term environmental safety of the SS-B stabilized soil with multiple high-concentration heavy metal contaminants." Ph.D. thesis, Southeast Univ., Nanjing, China (in Chinese).

Zhang, Z., et al. (2015). "Screening and assessment of solidification/stabilization amendments suitable for soils of lead-acid battery contaminated site." *J. Hazard. Mater.*, 288, 140–146.

Zhu, K., Yanagisawa, K., Onda, A., and Kajiyoshi, K. (2004). "Hydrothermal synthesis and morphology variation of cadmium hydroxyapatite." *J. Solid. State. Chem.*, 177(12), 4379–4385.